Monthly Notices of the ROYAL ASTRONOMICAL SOCIETY

MNRAS **468,** 4862–4871 (2017) doi:10.1093/mnras/stx670
Advance Access publication 2017 March 22

Disruption of sheet-like structures in Alfvénic turbulence by magnetic reconnection

A. Mallet,[1]★ A. A. Schekochihin[2,3] and B. D. G. Chandran[1]

[1]*Space Science Center, University of New Hampshire, Durham, NH 03824, USA*
[2]*Rudolf Peierls Centre for Theoretical Physics, University of Oxford, Oxford OX1 3NP, UK*
[3]*Merton College, Oxford OX1 4JD, UK*

Accepted 2017 March 15. Received 2017 February 19; in original form 2016 December 21

ABSTRACT

We propose a mechanism whereby the intense, sheet-like structures naturally formed by dynamically aligning Alfvénic turbulence are destroyed by magnetic reconnection at a scale $\hat{\lambda}_{\rm D}$, larger than the dissipation scale predicted by models of intermittent, dynamically aligning turbulence. The reconnection process proceeds in several stages: first, a linear tearing mode with N magnetic islands grows and saturates, and then the X-points between these islands collapse into secondary current sheets, which then reconnect until the original structure is destroyed. This effectively imposes an upper limit on the anisotropy of the structures within the perpendicular plane, which means that at scale $\hat{\lambda}_{\rm D}$ the turbulent dynamics change: at scales larger than $\hat{\lambda}_{\rm D}$, the turbulence exhibits scale-dependent dynamic alignment and a spectral index approximately equal to $-3/2$, while at scales smaller than $\hat{\lambda}_{\rm D}$, the turbulent structures undergo a succession of disruptions due to reconnection, limiting dynamic alignment, steepening the effective spectral index and changing the final dissipation scale. The scaling of $\hat{\lambda}_{\rm D}$ with the Lundquist (magnetic Reynolds) number $S_{\rm L_\perp}$ depends on the order of the statistics being considered, and on the specific model of intermittency; the transition between the two regimes in the energy spectrum is predicted at approximately $\hat{\lambda}_{\rm D} \sim S_{\rm L_\perp}^{-0.6}$. The spectral index below $\hat{\lambda}_{\rm D}$ is bounded between $-5/3$ and -2.3. The final dissipation scale is at $\hat{\lambda}_{\eta,\infty} \sim S_{\rm L_\perp}^{-3/4}$, the same as the Kolmogorov scale arising in theories of turbulence that do not involve scale-dependent dynamic alignment.

Key words: magnetic reconnection – MHD – turbulence – solar wind.

1 INTRODUCTION

Turbulence is thought to be important in many astrophysical situations, and is also measured directly by spacecraft in the solar wind (Bruno & Carbone 2013). In many situations, the system consists of an ionized plasma threaded by a strong mean magnetic field $\boldsymbol{B}_0$. In this case, the Alfvénically polarized fluctuations decouple from the compressive modes and satisfy the reduced magnetohydrodynamics (RMHD) equations (Strauss 1976), regardless of the collisionality of the plasma (Schekochihin et al. 2009). Written in terms of Elsasser (1950) variables $\boldsymbol{z}_\perp^\pm = \boldsymbol{u}_\perp \pm \boldsymbol{b}_\perp$, where $\boldsymbol{u}_\perp$ and $\boldsymbol{b}_\perp$ are the velocity and magnetic field (in velocity units) perturbations perpendicular to $\boldsymbol{B}_0$, these equations are

$$\partial_t \boldsymbol{z}_\perp^\pm \mp v_{\rm A}\partial_z \boldsymbol{z}_\perp^\pm + \boldsymbol{z}_\perp^\mp \cdot \nabla_\perp \boldsymbol{z}_\perp^\pm = -\nabla_\perp p, \qquad (1)$$

where the pressure p is obtained from the solenoidality condition $\nabla_\perp \cdot \boldsymbol{z}_\perp^\pm = 0$, the Alfvén speed is $v_{\rm A} = |\boldsymbol{B}_0|$ and $\boldsymbol{B}_0$ is in the z direction.

The turbulent system described by equation (1) has several interesting characteristics. First, it is anisotropic with respect to the direction of the local magnetic field, as attested by numerical simulations (Shebalin, Matthaeus & Montgomery 1983; Oughton, Dmitruk & Matthaeus 2004; Chen et al. 2011; Beresnyak 2015; Mallet et al. 2016) and solar-wind measurements (Horbury, Forman & Oughton 2008; Podesta 2009; Wicks et al. 2010; Chen et al. 2011; Chen 2016). This anisotropy can be understood in terms of the critical-balance conjecture (Goldreich & Sridhar 1995, 1997), whereby the linear (Alfvén) time $\tau_{\rm A} \sim l_\parallel/v_{\rm A}$ ($l_\parallel$ being the fluctuations' coherence length along the magnetic field line) and non-linear time $\tau_{\rm nl}$ should be similar to each other at all scales, $\tau_{\rm A} \sim \tau_{\rm nl}$.

Secondly, it has been noticed that at least in numerical simulations there is a tendency for the different fields $(\boldsymbol{z}_\perp^\pm, \boldsymbol{u}_\perp, \boldsymbol{b}_\perp)$ to *align* with one another within a small, scale-dependent angle θ

★E-mail: alfred.mallet@unh.edu

© 2017 The Authors
Published by Oxford University Press on behalf of the Royal Astronomical Society

(Boldyrev 2006, hereafter B06; Beresnyak & Lazarian 2006; Mason, Cattaneo & Boldyrev 2006). In the non-linear term in equation (1), only $z_\perp^\pm$ with a gradient in the direction of $z_\perp^\mp$ gives rise to a non-zero contribution. Combined with the solenoidality of the RMHD fields, this implies that the alignment causes the non-linearity to be noticeably suppressed. One can take this into account by defining the non-linear time as follows:

$$\tau_{\rm nl}^{\pm} \doteq \frac{\lambda}{\delta z_\perp^{\mp} \sin\theta}. \tag{2}$$

If $\sin\theta$ is scale dependent, it may affect how the fluctuation amplitudes $\delta z_\perp^\pm$ scale with the perpendicular scale λ. One can link the alignment effect to local anisotropy of the turbulent structures within the perpendicular plane. The aspect ratio of a sheet is related to the alignment angle between $\delta\boldsymbol{u}_\perp$ and $\delta\boldsymbol{b}_\perp$ fluctuations (see Boldyrev 2006) or between $\delta z_\perp^+$ and $\delta z_\perp^-$ fluctuations (see Chandran, Schekochihin & Mallet 2015) via

$$\frac{\lambda}{\xi} \sim \sin\theta, \tag{3}$$

where ξ is the coherence length of the structure in the direction of the vector fluctuations (hereafter the 'fluctuation-direction scale'), and λ is the coherence length of the structure in the direction perpendicular to this and also perpendicular to the parallel direction along the magnetic field (which we therefore call the 'perpendicular scale'). This 3D anisotropy has been measured in numerical simulations (Verdini & Grappin 2015; Mallet et al. 2016) and in the solar wind (Chen et al. 2012, although in the latter case, it has not as yet been definitively pronounced scale dependent).

The third key feature of Alfvénic turbulence, seen in both numerical simulations and in the solar wind, is its high degree of intermittency. Two related models of this intermittency that take into account both critical balance and dynamic alignment (Chandran et al. 2015; Mallet & Schekochihin 2017, reviewed in Section 2) show that, at each scale, higher amplitude fluctuations are systematically more aligned and therefore more anisotropic in the perpendicular plane. Anticorrelation of the alignment angle and amplitude has been confirmed in numerical simulations (Mallet, Schekochihin & Chandran 2015; Mallet et al. 2016).

Models of turbulence that incorporate dynamic alignment tend to predict perpendicular spectral indices close to $-3/2$ (Boldyrev 2006; Chandran et al. 2015; Mallet & Schekochihin 2017), while the original 'GS95' (Goldreich & Sridhar 1995) model, which does not include dynamic alignment, predicts a $-5/3$ spectral index. Surprisingly, which of these two classes of models is correct has still not been settled numerically: while spectral indices measured in extremely high-resolution ($2048^2 \times 512$) simulations are very close to $-3/2$ (Perez et al. 2012, 2014), the scaling of the dissipation scale λ_η with Reynolds number ($\mathrm{Re} \doteq L_\perp \delta z/\eta$, where η is the resistivity) in simulations with equivalent resolution appears to agree much better with the prediction using the GS95 model, $\lambda_\eta \propto \mathrm{Re}^{-3/4}$ (Beresnyak 2014). This suggests that there may be some small scale (perhaps relatively close to, but not smaller than, the dissipative scale predicted by the alignment theories) past which further alignment (or, equivalently, anisotropy within the perpendicular plane) breaks down.

In this paper, we propose a mechanism that causes the turbulent structures to stop aligning and becoming more sheet like. It appears to be in the nature of the turbulence, at least at large scales, to dynamically generate coherent, large amplitude, sheet-like structures. It is well known that sheet-like current structures are unstable to tearing modes[1] (Furth, Killeen & Rosenbluth 1963; Coppi et al. 1976), and that these modes can eventually disrupt the initial sheet-like structures via magnetic reconnection (Loureiro et al. 2005; Tenerani et al. 2016; Uzdensky & Loureiro 2016). This paper attempts to answer the question of whether and at what scale this process occurs for the kind of sheet-like structures that are dynamically formed by the aligning Alfvénic turbulence. It has recently been realized that, as current sheets form, they are violently unstable to the tearing instability, and so they never reach the idealized 'Sweet-Parker' reconnection regime (Parker 1957; Sweet 1958; Loureiro, Schekochihin & Cowley 2007; Pucci & Velli 2014; Tenerani et al. 2016; Uzdensky & Loureiro 2016) but instead break up into shorter sheets separated by magnetic islands. There are several stages in this process: the initial linear growth of the tearing instability, a possible Rutherford stage (Rutherford 1973) involving secular growth of the magnetic islands and, finally, collapse of the *X*-points between the islands into short, Sweet-Parker-like sheets, which disrupt the initial structure by magnetic reconnection (Loureiro et al. 2005). The characteristic time-scales of these processes, discussed in Section 3, make up the overall time needed to disrupt the sheet, which must be compared with the turbulent cascade time, $\tau_{\rm C} \sim \tau_{\rm nl} \sim \tau_{\rm A}$, to determine if the disruption occurs. This is done in Section 4. We then determine the critical scale below which the sheet-like structures cannot survive, and also determine the number of magnetic islands that the sheets are broken into (see Sections 4.4 and 5). We also discuss, in Section 6, the possible nature of the turbulence below the disruption scale, and show that the disruption process (repeated in a recursive fashion) leads to the Kolmogorov (1941) scaling of the final dissipative cutoff, and a steepening of the spectrum below the disruption scale. This can potentially explain the controversy between the results of Perez et al. (2014) and Beresnyak (2014), as well as being an interesting physical example of turbulence creating the conditions needed for reconnection.

2 TURBULENCE PHENOMENOLOGY

The intermittency models of Chandran et al. (2015, hereafter CSM15) and Mallet & Schekochihin (2017, hereafter MS17) both envision structures that are characterized by amplitude δz, and characteristic scales $l_\parallel$ (parallel scale), λ (perpendicular scale) and ξ (fluctuation-direction scale). Here, we outline the scalings arising from these models that we need in this work. Following MS17, we introduce normalized variables

$$\delta\hat{z} = \frac{\delta z}{\overline{\delta z}}, \quad \hat{\lambda} = \frac{\lambda}{L_\perp}, \quad \hat{l}_\parallel = \frac{l_\parallel}{L_\parallel}, \quad \hat{\xi} = \frac{\xi}{L_\perp}, \tag{4}$$

where $\overline{\delta z}$ is the outer-scale fluctuation amplitude, and $L_\perp$ and $L_\parallel$ are the perpendicular and parallel outer scales, respectively. The normalized amplitude in both models is given by $\delta\hat{z} \sim \beta^q$, where the non-negative random integer q is a Poisson random variable[2] with the mean $\mu = -\ln\hat{\lambda}$, and β is a dimensionless constant. This form for the distribution of the amplitude may be motivated by

[1] One might also ask whether these sheets could be disrupted by the Kelvin–Helmholtz instability. However, since the vortex stretching terms for the different Elsasser fields have opposite sign (Zhdankin, Boldyrev & Uzdensky 2016), in general, there will be more 'current sheets' than 'shear layers'. In such sheets, the Kelvin–Helmholtz instability is suppressed (Chandrasekhar 1961).

[2] Technically, in the MS17 model, the distribution of q conditional on $\hat{\lambda}$ is a Poisson mixture, which, however, gives the same scalings for the structure functions as would be obtained with a pure Poisson-distributed q.

modelling the amplitude as decreasing by a fixed factor β each time some quantized event (interpreted in CSM15 as a balanced collision) occurs, as the structure sharpens in scale (She & Waymire 1995). The perpendicular scalings are given in both models by

$$\langle \delta\hat{z}^m \rangle \sim \hat{\lambda}^{\zeta_m^\perp}, \tag{5}$$

with

$$\zeta_m^\perp = 1 - \beta^m, \tag{6}$$

where β is fixed via two different strategies in the two models: in MS17, the result is $\beta = 1/\sqrt{2}$, while in CSM15, $\beta = 0.691$. We will find it useful to define the 'effective amplitude' of the structures that dominate the mth order perpendicular structure function:

$$\langle \delta\hat{z}^m | \hat{\lambda} \rangle \equiv (\delta\hat{z}[m])^m \sim \hat{\lambda}^{1-\beta^m}, \tag{7}$$

and so

$$\delta\hat{z}[m] \sim \hat{\lambda}^{(1-\beta^m)/m}. \tag{8}$$

Note that $(1-\beta^m)/m$ is a strictly decreasing function of m, and so m is a useful proxy for the amplitude of the structures at a given scale. Three cases in particular will be important. The first is $m \to \infty$, corresponding to the most intense structures with $q = 0$, which have amplitudes

$$\delta\hat{z}[\infty] \sim 1, \tag{9}$$

independent of $\hat{\lambda}$. Secondly, $m = 2$ corresponds to the 'r.m.s. amplitude' structures that determine the spectral index (since this is simply related to the scaling of the second-order structure function), and have amplitudes

$$\delta\hat{z}[2] \sim \hat{\lambda}^{1/4}\,(\text{MS17}), \quad \delta\hat{z}[2] \sim \hat{\lambda}^{0.26}\,(\text{CSM15}). \tag{10}$$

Finally, the limit $m \to 0$ describes the 'bulk' fluctuations with $q = \mu$, whose amplitudes are

$$\delta\hat{z}[0] \sim \hat{\lambda}^{-\ln\beta}. \tag{11}$$

In both models, the fluctuation-direction scale $\hat{\xi}$ is given by

$$\hat{\xi} \sim \hat{\lambda}^\alpha \delta\hat{z}, \tag{12}$$

and the cascade time is

$$\tau_C \sim \tau_{nl} \sim \hat{\lambda}^{\kappa_1} \delta\hat{z}^{\kappa_2} \frac{L_\perp}{\delta z}. \tag{13}$$

In the MS17 model,

$$\alpha = \kappa_1 = 1/2, \quad \kappa_2 = 0, \tag{14}$$

while in the CSM15 model[3],

$$\alpha = 1 + \ln\beta, \quad \kappa_1 = (1+\ln\beta)^2, \quad \kappa_2 = 1 + \ln\beta. \tag{15}$$

Both models envision structures that are sheet-like in the perpendicular plane, with length ξ and width λ, satisfying $\xi \gg \lambda$. Note that taking $m = 2$ in the MS17 model recovers all the scalings of the original dynamic-alignment model due to Boldyrev (2006, which we will hereafter refer to as B06), but via a different derivation, and positing alignment between Elsasser fields rather than between the velocity and magnetic field. We will assume that the magnetic field varies by $\delta B \sim \delta z$ across the sheet, and further assume that any velocity fluctuation $\delta u \lesssim \delta B$ across the sheet[4] does not significantly alter the scalings of the tearing instability or its saturation. To determine whether and how structures of a particular amplitude are disrupted faster than they cascade, we must take a detailed look at the different time-scales involved in the disruption process.

[3] CSM15 defined the quantity ξ (or ξ_λ in their notation) to be the characteristic distance along the (δz^+) fluctuation direction that a weak δz^- fluctuation would propagate within an intense δz^+ sheet before exiting that sheet. CSM15 also showed (see e.g. their section 2.6) that two locations within a δz^+ sheet that are separated along the fluctuation direction by a distance $\sim\xi_\lambda$ cascade in different and uncorrelated ways. As a sheet-like δz^+ structure cascades to smaller scales, its characteristic dimension along the fluctuation direction in the CSM15 model thus becomes $\sim\xi_\lambda$.

3 TIMESCALES

The process whereby a sheet of length ξ and width λ, with a magnetic field jump $\delta B \sim \delta z$, can be destroyed by reconnection occurs in several stages, which we will now briefly review, following Uzdensky & Loureiro (2016). First, there is exponential growth of the linear tearing mode until the width of the island(s) is approximately the width of the inner layer where resistivity is important,

$$w \sim \delta_{in} \sim \left[\gamma (k\delta z)^{-2} \lambda^2 \eta\right]^{1/4}, \tag{16}$$

where γ is the linear growth rate of the tearing mode and $k \sim N/\xi$ is its wavenumber (N is the number of islands). Secondly, there may be secular "Rutherford' growth of the islands until $w \sim 1/\Delta'$, where Δ' is the instability parameter for the tearing mode. Thirdly, the X-point(s) that have arisen collapse into thin sheets, which then undergo fast reconnection, leaving behind a set of magnetic islands. We will examine these processes to determine which of them dominates the total time to disrupt the sheet, and thus determine whether this is faster than the cascade time τ_C.

3.1 Linear growth stage

We will assume that a typical sheet-like structure arising in dynamically aligning turbulence is reasonably well modelled by a Harris (1962) sheet, so

$$\Delta'\lambda = 2\left(\frac{1}{k\lambda} - k\lambda\right). \tag{17}$$

There is an instability provided that $\Delta' > 0$. We are interested in long-wavelength modes, so

$$\Delta'\lambda \sim \frac{1}{k\lambda} \sim \frac{\hat{\xi}}{N\hat{\lambda}}. \tag{18}$$

There are two possible situations: (i) $\Delta'\delta_{in} \ll 1$, 'FKR' modes (Furth et al. 1963) with

$$\gamma_{FKR} \sim \Delta'^{4/5} k^{2/5} \delta z^{2/5} \lambda^{-2/5} \eta^{3/5} \sim N^{-2/5} \left(\frac{\xi}{\lambda}\right)^{2/5} S_\lambda^{-3/5} \frac{\delta z}{\lambda}, \tag{19}$$

and (ii) $\Delta'\delta_{in} \sim 1$, 'Coppi' modes (Coppi et al. 1976) with

$$\gamma_{Coppi} \sim k^{2/3} \delta z^{2/3} \lambda^{-2/3} \eta^{1/3} \sim N^{2/3} \left(\frac{\xi}{\lambda}\right)^{-2/3} S_\lambda^{-1/3} \frac{\delta z}{\lambda}, \tag{20}$$

[4] The '$\lesssim$' is important because for $\delta u > \delta B$, the Kelvin–Helmholtz mode dominates over the tearing mode. However, we neglect this situation for the reasons given in footnote 1.

where the Lundquist number[5] is $S_\lambda \doteq \lambda \delta z/\eta$. Since these two modes have opposite dependence on k, the maximum growth rate can be found at the wavenumber where $\gamma_{\rm FKR} \sim \gamma_{\rm Coppi}$, giving

$$k_{\max}\lambda \sim S_\lambda^{-1/4}, \quad \gamma_{\max} \sim S_\lambda^{-1/2}\frac{\delta z}{\lambda}. \tag{21}$$

However, this 'transitional mode' is only accessible if it actually fits into the sheet, i.e. if

$$k_{\max}\xi \sim N_{\max} \sim \frac{\hat{\xi}}{\hat{\lambda}} S_\lambda^{-1/4} > 1. \tag{22}$$

The maximum growth rate for a particular structure is thus either $\gamma_{\max}$ given by equation (21), if $k_{\max}$ fits into the structure, or $\gamma_{\rm FKR}$ given by equation (19) with $N = 1$, the longest-wavelength FKR mode, otherwise.

3.2 Rutherford growth stage

The linear growth stage ends when the width of the islands $w \sim \delta_{\rm in}$, given by equation (16). If $\Delta' w \ll 1$, there will be secular 'Rutherford' growth (Rutherford 1973) until $\Delta' w \sim 1$,

$$w \sim \eta \Delta' t. \tag{23}$$

If present, this stage lasts for a time

$$\tau_{\rm Ruth} \sim \frac{1}{\eta \Delta'^2} \sim N^2 \left(\frac{\hat{\lambda}}{\hat{\xi}}\right)^2 S_\lambda \frac{\lambda}{\delta z}. \tag{24}$$

Note that $\tau_{\rm Ruth}$ increases with N, so if the maximum growth rate is attained for the $N = 1$ FKR mode, this mode will also exit the Rutherford stage and saturate first. In the FKR limit, $\Delta' \delta_{\rm in} \ll 1$, and so there is a well-defined Rutherford stage. For the Coppi modes, $\Delta' \delta_{\rm in} \sim 1$, and so there is no Rutherford stage.

3.3 Collapse/reconnection stage

At the end of the Rutherford stage (or immediately after the linear stage in the case of Coppi modes), the X-point(s) formed by the tearing mode collapse into thin secondary sheets, each of length $\sim \xi/N$, and reconnect the flux in the original structure. This collapse, studied by Loureiro et al. (2005), results in exponential, Sweet-Parker-like growth of the reconnected flux on a time-scale that, written in terms of our variables, is

$$\gamma_{\rm SP} \sim S_\lambda^{-1/2}\frac{\delta \hat{z}}{\lambda} \sim \gamma_{\max}, \tag{25}$$

and so the rate of the collapse is always greater than or equal to the growth rate of the initial linear instability. Following Uzdensky & Loureiro (2016), we therefore do not need to consider the time associated with this stage in our determination of the disruption time of the original structure.

For high enough $S_{\rm L_\perp}$, the collapse rate becomes independent of S_λ because the Lundquist number associated with the secondary sheets becomes larger than $S_{\rm c} \sim 10^4$, the critical Lundquist number required to trigger the onset of plasmoid-dominated fast reconnection (Loureiro, Schekochihin & Cowley 2007; Bhattacharjee et al. 2009; Samtaney et al. 2009; Uzdensky, Loureiro & Schekochihin 2010; Loureiro et al. 2012). The critical $S_{\rm L_\perp}$ necessary to access the plasmoid-dominated regime will be determined in Section 4.5.

[5] Note that S_λ is just what in turbulence theory one would usually call the local magnetic Reynolds number at scale λ.

3.4 Disruption time

Based on the above scalings, we can now identify the disruption time as

$$\tau_{\rm D} \sim \begin{cases} \max[1/\gamma_{\rm FKR}, \tau_{\rm Ruth}] & \text{if } \hat{\lambda} > \hat{\lambda}_{\rm tr}, \\ 1/\gamma_{\max} & \text{if } \hat{\lambda} \le \hat{\lambda}_{\rm tr}. \end{cases} \tag{26}$$

This is just restating the key result of Uzdensky & Loureiro (2016), which will allow us to compare $\tau_{\rm D}$ with the cascade time $\tau_{\rm C}$. The transition scale $\hat{\lambda}_{\rm tr}$ will be worked out in Section 4.2.

3.5 Resistive time

If the structures are not able to be disrupted by reconnection, they can simply decay resistively on a time-scale

$$\tau_\eta \sim \frac{\lambda^2}{\eta}. \tag{27}$$

The interesting question that we will answer in this paper is whether and under what circumstances this basic dissipation mechanism is superceded by tearing and the onset of reconnection.

4 CRITICAL SCALES

In this section, we will calculate the critical scales that partition the domain defined by $\hat{\lambda}$ and m (see equation 8) into regions where the structures are and they are not disrupted by the onset of reconnection. To do this, we need to compare the time-scales identified in Section 3 to the cascade time $\tau_{\rm C}$ (equation 13).

4.1 Resistive scale

First, we deal with the dissipative scale for the turbulence in the absence of any disruption by reconnection. Using equations (13) and (27), we evaluate

$$\frac{\tau_{\rm C}}{\tau_\eta} \sim \frac{\hat{\lambda}^{\kappa_1}\delta\hat{z}^{\kappa_2} L_\perp \eta}{\lambda^2 \delta z} \sim \hat{\lambda}^{\kappa_1 - 2}\delta\hat{z}^{\kappa_2} S_{\rm L_\perp}^{-1}. \tag{28}$$

We consider fluctuations $\delta\hat{z}[m]$ that are important for the mth-order structure function, using equation (8), to obtain

$$\frac{\tau_{\rm C}}{\tau_\eta} \sim S_{\rm L_\perp}^{-1}\hat{\lambda}^{\kappa_1 - 2 + \kappa_2 \zeta_m^\perp/m}. \tag{29}$$

Therefore, the resistive scale for these mth-order structures is

$$\hat{\lambda}_\eta \sim S_{\rm L_\perp}^{-(2-\kappa_1-\kappa_2\zeta_m^\perp/m)^{-1}}. \tag{30}$$

In the MS17 model, since $\kappa_1 = 1/2$ and $\kappa_2 = 0$,

$$\hat{\lambda}_\eta^{\rm MS} \sim S_{\rm L_\perp}^{-2/3}, \tag{31}$$

independent of m. This is the standard estimate for the dissipation scale (the analogue of the Kolmogorov scale) in the original dynamic-alignment model of B06 (see e.g. Perez et al. 2012 for an explicit derivation of this scaling). In the CSM15 model,

$$\hat{\lambda}_\eta^{\rm CSM} \sim S_{\rm L_\perp}^{-\left(1.60-0.63\zeta_m^\perp/m\right)^{-1}}, \tag{32}$$

so the low-order, lower amplitude fluctuations dissipate at smaller scales than the high-order, higher amplitude fluctuations.

4.2 Boundary between FKR and transitional modes

The boundary between the two different regimes for the linear tearing stage is given by equation (22), $S_\lambda^{-1/4}\hat{\xi}/\hat{\lambda} \sim 1$. Using

equation (12) and replacing $\delta\hat{z}$ with the typical amplitude of an mth-order structure given by equation (8), we see that the transitional mode (21) may only occur when

$$\hat{\lambda} < \hat{\lambda}_{\rm tr} \sim S_{\rm L_\perp}^{1/4\left(\alpha-\frac{5}{4}+\frac{3}{4}\frac{\zeta_m^\perp}{m}\right)^{-1}}. \tag{33}$$

In the MS17 model,

$$\hat{\lambda}_{\rm tr}^{\rm MS} \sim S_{\rm L_\perp}^{-1/3(1-\zeta_m^\perp/m)^{-1}}, \tag{34}$$

while in the CSM15 model,

$$\hat{\lambda}_{\rm tr}^{\rm CSM} \sim S_{\rm L_\perp}^{-0.40(1-1.21\zeta_m^\perp/m)^{-1}}. \tag{35}$$

At scales $\hat{\lambda} > \hat{\lambda}_{\rm tr}$, the FKR mode with $N = 1$ is the most unstable linear mode, while at $\hat{\lambda} < \hat{\lambda}_{\rm tr}$, the transitional mode (21) is the fastest.

4.3 Linear FKR critical scale

To determine whether the $N = 1$ FKR mode grows fast enough to disrupt the structures, we first calculate, using equations (8), (12), (13) and (19),

$$\begin{aligned}\gamma_{\rm FKR}[N=1]\tau_{\rm C} &\sim \left(\frac{\hat{\xi}}{\hat{\lambda}}\right)^{2/5} S_\lambda^{-3/5}\frac{\delta\hat{z}}{\hat{\lambda}}\hat{\lambda}^{\kappa_1}\delta\hat{z}^{\kappa_2}\\ &\sim S_{\rm L_\perp}^{-3/5}\hat{\lambda}^{\frac{2\alpha}{5}-2+\kappa_1}\delta\hat{z}^{\frac{4}{5}+\kappa_2}\\ &\sim S_{\rm L_\perp}^{-3/5}\hat{\lambda}^{\frac{2\alpha}{5}-2+\kappa_1+\frac{\zeta_m^\perp}{m}\left(\frac{4}{5}+\kappa_2\right)}.\end{aligned} \tag{36}$$

The sheet will not be disrupted unless $\gamma_{\rm FKR}[N=1]\tau_{\rm C} > 1$. This is equivalent to

$$\hat{\lambda} < \hat{\lambda}_{\rm FKR} \sim S_{\rm L_\perp}^{3/5\left[\frac{2\alpha}{5}-2+\kappa_1+\frac{\zeta_m^\perp}{m}\left(\frac{4}{5}+\kappa_2\right)\right]^{-1}}. \tag{37}$$

For the MS17 model,

$$\hat{\lambda}_{\rm FKR}^{\rm MS} \sim S_{\rm L_\perp}^{-6/13\left(1-\frac{8\zeta_m^\perp}{13m}\right)^{-1}}, \tag{38}$$

while for the CSM15 model,

$$\hat{\lambda}_{\rm FKR}^{\rm CSM} \sim S_{\rm L_\perp}^{-0.44(1-1.06\zeta_m^\perp/m)^{-1}}. \tag{39}$$

Comparing these scalings with equation (33), we see that the scale $\hat{\lambda}_{\rm FKR}$ is smaller than the corresponding $\hat{\lambda}_{\rm tr}$ for all m, and so there are no FKR modes that grow fast enough to disrupt the structures. Therefore, we do not need to consider the duration of the Rutherford stage (see Section 3.2) to determine whether disruption occurs.

4.4 Disruption scale

For a given m, at $\hat{\lambda} \le \hat{\lambda}_{\rm tr}$, with the latter scale given by equation (33), the disruption time is, therefore,

$$\tau_{\rm D} \sim 1/\gamma_{\rm max}, \tag{40}$$

and we must calculate

$$\begin{aligned}\gamma_{\rm max}\tau_{\rm C} &\sim S_\lambda^{-1/2}\frac{\delta\hat{z}}{\hat{\lambda}}\hat{\lambda}^{\kappa_1}\delta\hat{z}^{\kappa_2}\\ &\sim \hat{\lambda}^{-3/2+\kappa_1+(1/2+\kappa_2)\zeta_m^\perp/m}S_{\rm L_\perp}^{-1/2},\end{aligned} \tag{41}$$

where we have used equation (21) for $\gamma_{\rm max}$ and equations (8) and (13) to express $\tau_{\rm C}$ and $\delta\hat{z}$ in terms of $\hat{\lambda}$ and m. The sheet will be disrupted if $\gamma_{\rm max}\tau_{\rm C} > 1$. This happens for

$$\hat{\lambda} < \hat{\lambda}_{\rm D} \sim S_{\rm L_\perp}^{-1/2\left[\frac{3}{2}-\kappa_1-\left(\frac{1}{2}+\kappa_2\right)\frac{\zeta_m^\perp}{m}\right]^{-1}}. \tag{42}$$

The corresponding number of islands, from equation (22), is

$$\begin{aligned}N_{\rm D} &\sim S_{\lambda_{\rm D}}^{-1/4}\frac{\hat{\xi}_{\rm D}}{\hat{\lambda}_{\rm D}},\\ &\sim \hat{\lambda}_{\rm D}^{\alpha-5/4+3\zeta_m^\perp/4m}S_{\rm L_\perp}^{-1/4},\\ &\sim S_{\rm L_\perp}^{\left\{\frac{1}{2}\left(\frac{5}{4}-\alpha-\frac{3\zeta_m^\perp}{4m}\right)\left[\frac{3}{2}-\kappa_1-\left(\frac{1}{2}+\kappa_2\right)\frac{\zeta_m^\perp}{m}\right]^{-1}-\frac{1}{4}\right\}}.\end{aligned} \tag{43}$$

In the MS17 model, these scalings become

$$\hat{\lambda}_{\rm D}^{\rm MS} \sim S_{\rm L_\perp}^{-1/2\left(1-\frac{\zeta_m^\perp}{2m}\right)^{-1}}, \quad N_{\rm D}^{\rm MS} \sim S_{\rm L_\perp}^{\frac{1-2\zeta_m^\perp/m}{8-4\zeta_m^\perp/m}}, \tag{44}$$

while in the CSM15 model,

$$\hat{\lambda}_{\rm D}^{\rm CSM} \sim S_{\rm L_\perp}^{-0.45\left(1-1.03\zeta_m^\perp/m\right)^{-1}}, \quad N_{\rm D}^{\rm CSM} \sim S_{\rm L_\perp}^{\frac{1-2.71\zeta_m^\perp/m}{32.3-32.1\zeta_m^\perp/m}}. \tag{45}$$

Note that $\hat{\lambda}_{\rm D} < \hat{\lambda}_{\rm tr}$, as expected, since no FKR modes grow fast enough to disrupt the sheets (see Section 4.3). These scalings determine the largest $\hat{\lambda}$ for which the fastest growing mode reaches collapse in a time shorter than the cascade time $\tau_{\rm C}$ of the turbulence, and, therefore, the smallest $\hat{\lambda}$ for which the aligned, sheet-like structures can survive. We will examine some instructive particular cases and the physical consequences of these results in Sections 5 and 6.

4.5 Critical $S_{\rm L_\perp}$ for the plasmoid-dominated regime

As an interesting aside, we noted in Section 3.3 that for high enough $S_{\rm L_\perp}$ the reconnection rate $\gamma_{\rm SP}$ becomes independent of S_λ due to the onset of the plasmoid instability. For this to occur, the Lundquist number associated with the secondary sheets must be

$$S_{\xi_{\rm D}/N_{\rm D}} \sim \hat{\lambda}_{\rm D}\delta\hat{z}_{\hat{\lambda}_{\rm D}}S_{\hat{\lambda}_{\rm D}}^{1/4}S_{\rm L_\perp} \sim \hat{\lambda}_{\rm D}^{5/4\left(1+\zeta_m^\perp/m\right)}S_{\rm L_\perp}^{5/4} > S_{\rm c}, \tag{46}$$

where we used equation (22) for $N_{\rm D} = N_{\rm max}$. Expressing this condition in terms of $S_{\rm L_\perp}$, we obtain in the MS17 model, using equation (44),

$$S_{\rm L_\perp} > S_{\rm c}^{4/5\frac{1-\zeta_m^\perp/2m}{1/2-\zeta_m^\perp/m}}. \tag{47}$$

In the CSM15 model, we obtain

$$S_{\rm L_\perp} > S_{\rm c}^{\frac{1.47-1.51\zeta_m^\perp/m}{1-2.72\zeta_m^\perp/m}}. \tag{48}$$

For such values of $S_{\rm L_\perp}$, the secondary sheets will break into plasmoids and the reconnection/collapse rate will be given by

$$\gamma_{\rm plasmoids} \sim S_{\rm c}^{-1/2}\frac{\delta\hat{z}}{\lambda}, \tag{49}$$

instead of equation (25), because the secondary sheet will be broken into 'critical Sweet-Parker sheets' (Uzdensky et al. 2010), each of which will reconnect at this rate. Assuming $S_{\rm c} \sim 10^4$ (Loureiro et al. 2007; Samtaney et al. 2009),[6] the critical $S_{\rm L_\perp}$ given by equation (47) is quite high: for the $m = \infty$ structures in the MS17

[6] Note that in a turbulent environment, $S_{\rm c}$ may be somewhat lower, possibly by as much as an order of magnitude (see Loureiro et al. 2009).

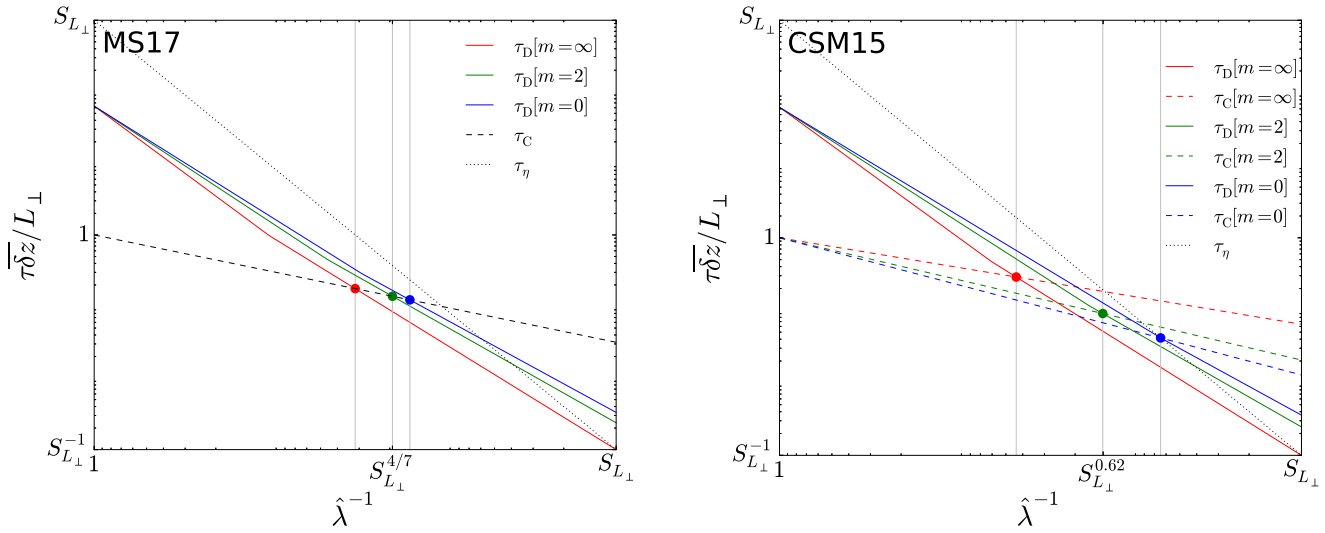

Figure 1. Comparison of the cascade time-scale τ_C, equation (13, dashed lines), the disruption time-scale τ_D, equation (26, solid, coloured lines) and the resistive time-scale τ_η, equation (27, dotted lines), for the MS17 model (left-hand panel) and the CSM15 panel (right-hand panel). Where these time-scales depend on the order m of the fluctuations, three values of m are plotted: $m = \infty$ (in red), $m = 2$ (in green) and $m = 0$ (in blue). In the CSM15 model, not only τ_D but also the cascade time varies with m, and so there are three curves for τ_C. In the MS17 model, τ_C does not depend on m, and so there is a single curve. The point at which the disruption process becomes faster than the turbulent cascade is marked with a circle for each m, and a grey vertical line marks the corresponding scale $\hat{\lambda}_D[m]$, given by equations (44) for MS17 and (45) for CSM15.

model to be plasmoid unstable, $S_{L_\perp} \gtrsim S_c^{8/5} \sim 10^6$, while for the $m = 2$ structures in the MS17 model, $S_{L_\perp} \gtrsim S_c^{14/5} \sim 10^{11}$. In the CSM15 model, the $m = \infty$ structures are plasmoid unstable for $S_{L_\perp} \gtrsim S_c^{1.47} \sim 10^6$, while the $m = 2$ structures are plasmoid unstable for $S_{L_\perp} \gtrsim S_c^{3.7} \sim 10^{15}$. This suggests that the plasmoid-dominated regime is not accessible in current numerical simulations, as indeed confirmed by the absence of plasmoid-unstable current sheets in the simulations of Zhdankin et al. (2013). The critical $S_{L_\perp}$ is much higher than the critical Lundquist number for a Sweet-Parker sheet to be plasmoid unstable because the structures formed by the turbulence do not have a particularly high aspect ratio. The mechanism outlined in this paper does not rely on the secondary sheets being plasmoid unstable. For the disruption to occur, we only need $\tau_C/\tau_D > 1$, where τ_D is set by the tearing growth rate.

5 TRANSITION TO A NEW REGIME OF STRONG ALFVÉNIC TURBULENCE

The comparison of time-scales in Section 4 has allowed us to predict the scale at which the sheet-like structures at each order m are disrupted by the onset of reconnection. While the cascade time τ_C (equation 13)) decreases as the cascade progresses to smaller scales, so does the disruption time τ_D (equation 26). Since the non-linearity in the aligned sheet-like structures is suppressed by a factor equal to their alignment angle (inverse aspect ratio), τ_D decreases faster than the cascade time, and eventually becomes smaller, at the scale $\hat{\lambda}_D$. This is shown in Fig. 1 for both the MS17 and CSM15 models, for $m = \infty$, 2, 0 (most intense, rms. amplitude and most typical structures, respectively). Also shown are the disruption scales $\hat{\lambda}_D[m]$ beyond which the sheet-like structures of order m cannot survive.

The effect that the disruption has on the turbulence is, thus, as follows: for $\hat{\lambda} < \hat{\lambda}_D$, the sheet-like structures predicted by the turbulence models that rely on dynamic alignment (e.g. MS17, CSM15 and the original model of B06) are disrupted by reconnection into several separate islands. The detailed dependence of $\hat{\lambda}_D$ on m in the MS17 and CSM15 models (equations 44 and 45, respectively) is shown in Fig. 2, along with the resistive scales corresponding to these models (equations 31 and 32). The disruption scale $\hat{\lambda}_D$ is an increasing function of m. Roughly speaking, one might expect the behaviour of the mth-order structure function to change at $\hat{\lambda}_D[m]$. In practice, since structures of all orders contribute to all structure functions to differing degrees, the transition will take place over a range of scales between $\hat{\lambda}_D[\infty]$ and $\hat{\lambda}_D[0]$. As $m \to \infty$, the disruption scale approaches

$$\hat{\lambda}_D^{MS}[\infty] \sim S_{L_\perp}^{-1/2}, \quad \hat{\lambda}_D^{CSM}[\infty] \sim S_{L_\perp}^{-0.45}, \tag{50}$$

in the MS17 and CSM15 models, respectively. One might expect to see a change in the spectral index (since this is related to the scaling exponent of the second-order structure function) at around

$$\hat{\lambda}_D^{MS}[2] \sim S_{L_\perp}^{-4/7}, \quad \hat{\lambda}_D^{CSM}[2] \sim S_{L_\perp}^{-0.62}. \tag{51}$$

For $m = 0$ structures, the disruption scale is given by

$$\hat{\lambda}_D^{MS}[0] \sim S_{L_\perp}^{-0.60}, \quad \hat{\lambda}_D^{CSM}[0] \sim S_{L_\perp}^{0.73}. \tag{52}$$

In the MS17 model, the disruption scale is above the resistive scale for all m, $\hat{\lambda}_D > \hat{\lambda}_\eta$ (see Section 4.1). In the CSM15 model, $\hat{\lambda}_D > \hat{\lambda}_\eta$ for all $m > 0$, but $\hat{\lambda}_D[0]$ and $\hat{\lambda}_\eta[0]$ are identical. Thus, in the CSM15 model, $m = 0$ structures, which are neither aligned nor sheet like, cascade to their resistive scale without being disrupted by the onset of reconnection. This explicitly shows that the suppression of the non-linearity due to dynamic alignment is required for the disruption process to become effective at a larger scale than $\hat{\lambda}_\eta$.

6 TURBULENCE BELOW $\hat{\lambda}_D$

It is natural to ask what happens to the turbulence below the disruption scale $\hat{\lambda}_D$. We will restrict ourselves to the case of $m = 2$ (the r.m.s. amplitude structures) for the following discussion, i.e. we forgo any discussion of intermittency below $\hat{\lambda}_D$.

We expect the sheet-like structures just above $\hat{\lambda}_D$ to be broken up into 'flux-rope-like' structures (3D versions of plasmoids) just

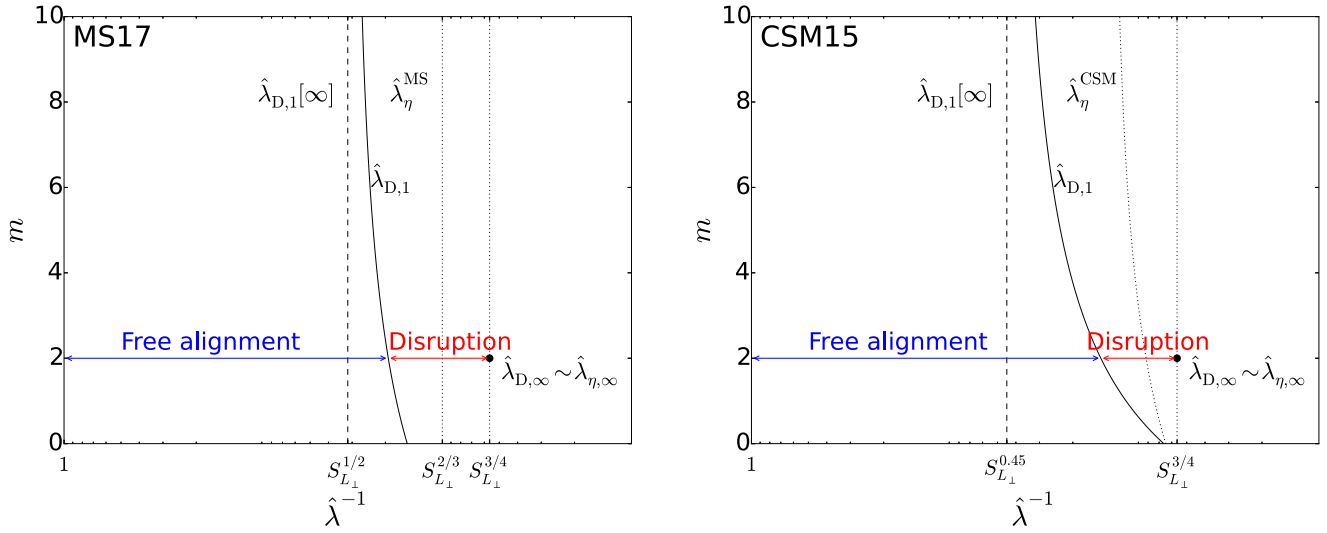

Figure 2. The solid black line shows the dependence of $\hat{\lambda}_{\mathrm{D},1}$ on m in the MS17 model (equation 44, left-hand panel) and in the CSM15 model (equation 45, right-hand panel). The dashed lines show $\hat{\lambda}_{\mathrm{D},1}[m=\infty]$. The two different subranges for the $m=2$ structures are marked by blue and red arrows. The leftmost (i.e. larger scale) dotted line in each plot shows the expected dissipation scales (31) and (32) of the Alfvénic turbulence without disruption, while the rightmost (smaller scale) dotted line shows the Kolmogorov scale, $S_{\mathrm{L}_\perp}^{-3/4}$. The black point shows the value of the final dissipation scale of the disrupted turbulence $\hat{\lambda}_{\mathrm{D},\infty} \sim \hat{\lambda}_{\eta,\infty}$ (equations 60 and 63), equal to the Kolmogorov scale.

below $\hat{\lambda}_{\mathrm{D}}$: these are roughly circular in the perpendicular plane, with scale $\hat{\lambda}_{\mathrm{D}}$,[7] but extended in the direction parallel to the local magnetic field, due to critical balance. These structures, no longer anisotropic in the perpendicular plane, will break up non-linearly, serving as the energy-containing 'eddies' of a new cascade.

This implies that the fluctuation amplitude just below $\hat{\lambda}_{\mathrm{D}}$ should decrease[8]. Indeed, the energy flux just below the scale $\hat{\lambda}_{\mathrm{D}}$ must be equal to the energy flux just above it, or at any other scale in the inertial range:

$$\epsilon \sim \frac{\overline{\delta z}^3}{L_\perp} \sim \frac{\delta z_{1,-}^3}{\lambda_{\mathrm{D}}}, \tag{53}$$

where $\delta z_{1,-}$ is the amplitude of the new structures. This gives a simple expression for this dynamically adjusted amplitude:

$$\delta\hat{z}_{1,-} \sim \hat{\lambda}_{\mathrm{D}}^{1/3}, \tag{54}$$

where we have normalized by outer-scale quantities in the usual way (4). We have assumed here that the reconnection process involved in the X-point collapse and formation of flux ropes (plasmoids) can be viewed as mostly transferring energy from one form of magnetic/velocity perturbation at scale λ_{D} (aligned structures) to another form of perturbation at scale λ_{D} (plasmoids, outflows). Moreover, since the cascade time-scale $\lambda_{\mathrm{D}}/\delta z_{1,-}$ for unaligned structures just below scale λ_{D} is shorter than the disruption time-scale, we assume that non-linear interactions between unaligned structures are the dominant mechanism for transferring fluctuation energy from scale λ_{D} to smaller scales. If a constant energy flux across $\hat{\lambda}_{\mathrm{D}}$ were not a good assumption, the amplitude below $\hat{\lambda}_{\mathrm{D}}$ would be smaller than that in equation (54), and the corresponding spectral slope at scales below $\hat{\lambda}_{\mathrm{D}}$ would be steeper than deduced in Section 6.3.

We expect the new structures to behave as they normally would in Alfvénic turbulence: to interact, cascade to smaller scales and dynamically align as the scale decreases. The change compared to the 'primary cascade' is that the disruption process effectively resets the perpendicular anisotropy at scale $\hat{\lambda}_{\mathrm{D}}$, so the aligning structures have smaller aspect ratios than they would have had without the disruption. The amplitude of the ($m=2$) turbulent structures at scales $\hat{\lambda} < \hat{\lambda}_{\mathrm{D}}$ scales as

$$\delta\hat{z} \sim \hat{\lambda}_{\mathrm{D}}^{1/3} \left(\hat{\lambda}/\hat{\lambda}_{\mathrm{D}}\right)^{\zeta_2^\perp/2}, \tag{55}$$

where $\zeta_2^\perp = 1/2$ in the MS17 model (and also in the original B06 theory) and $\zeta_2^\perp = 0.52$ in the CSM15 model.

These structures will eventually, in turn, be disrupted at a secondary disruption scale, have their amplitude dynamically adjusted to keep the energy flux constant and their perpendicular anisotropy removed, engendering another 'mini-cascade', and so on. Therefore, what we have so far called $\hat{\lambda}_{\mathrm{D}}$ is only the first of many subsequent disruption scales – and so from now on, we will call this first disruption scale $\hat{\lambda}_{\mathrm{D},1}$. We can therefore identify two distinct subranges of MHD turbulence:

$\hat{\lambda} > \hat{\lambda}_{\mathrm{D},1}$, 'free alignment range',
$\hat{\lambda} < \hat{\lambda}_{\mathrm{D},1}$, 'disruption range'.

The two subranges are shown in Fig. 2. We now proceed to discuss the sequence of disruptions (Section 6.1), the dissipation scale $\hat{\lambda}_{\eta,\infty}$ (Section 6.2) and the spectral index in the disruption range (Section 6.3).

6.1 Recursive disruption

The series of consecutive disruptions can be understood as follows. After the $(i-1)$st disruption, the turbulence behaves as though there is an ith cascade, with 'outer-scale' values of the turbulent variables

[7] Based on the numerical evidence in Loureiro et al. (2005), this does appear to be how the tearing mode saturates at high enough Δ'.

[8] This does not mean that there are actually sharp jumps in the structure function. As the cascade progresses to smaller scales, the fraction of the energy contained in disrupted structures increases continuously: the disruption scale is just the scale at which a given structure function is dominated by disrupted structures.

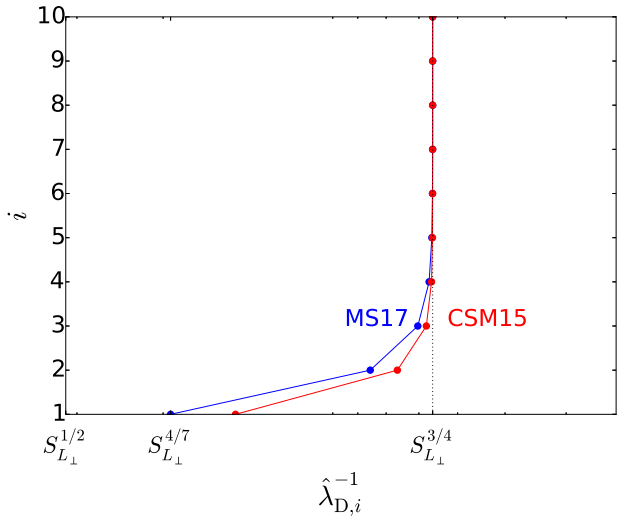

Figure 3. The dependence of $\hat{\lambda}_{D,i}$ on i (equation 59) is shown for the MS17 model (blue) and for the CSM15 model (red). The Kolmogorov scale given by equation (63) is shown as a black dotted line.

given by the values at the $(i-1)$st disruption scale, $\hat{\lambda}_{D,i-1}$. The cascade has the same scalings as the original cascade, but with the replacements

$$L_\perp \to \lambda_{D,i-1}, \quad \overline{\delta z} \to \delta z_{i-1,-} \sim \hat{\lambda}_{D,i-1}^{1/3}\overline{\delta z}, \tag{56}$$

in all places where either of these variables appear (including normalizations). Using the rule (56) in equations (44) and (45) for $\hat{\lambda}_D$ leads to the recursive relation

$$\hat{\lambda}_{D,i} \sim \hat{\lambda}_{D,i-1}^{1+4f_D/3} S_{L_\perp}^{f_D}. \tag{57}$$

This scale has been normalized by $L_\perp$ after performing the replacement procedure (56). The exponent f_D depends on the choice of turbulence model, and is the exponent in equation (51):

$$f_D = \begin{cases} -4/7, & \text{MS17 and B06 models,} \\ -0.62, & \text{CSM15 model.} \end{cases} \tag{58}$$

The recursion relation (57) may be written as

$$\hat{\lambda}_{D,i} \sim S_{L_\perp}^{f_D \sum_{j=0}^{i-1}[1+4f_D/3]^j}. \tag{59}$$

As $i \to \infty$, we have

$$\hat{\lambda}_{D,\infty} \sim S_{L_\perp}^{-3/4}. \tag{60}$$

Fig. 3 shows the scale $\hat{\lambda}_{D,i}$, for $i = 1, 2, 3, \ldots, 10$. Obviously, as i increases, the successive disruptions become ever closer to each other in scale, and so the disruption scale quickly approaches the asymptotic value (60).

6.2 Final dissipative cutoff scale

Similar to equation (57), using the rule (56) in equations (31) and (32) for $\hat{\lambda}_\eta$ leads to the recursive relation

$$\hat{\lambda}_{\eta,i} \sim \hat{\lambda}_{D,i-1}^{1+4f_\eta/3} S_{L_\perp}^{f_\eta}, \tag{61}$$

where the exponent f_η is given by the exponents of equation (31) or (32):

$$f_\eta = \begin{cases} -2/3, & \text{MS17 and B06 models,} \\ -0.70, & \text{CSM15 model, m} = 2. \end{cases} \tag{62}$$

The limit of $\hat{\lambda}_{\eta,i}$ as $i \to \infty$ is also given by (60), so

$$\hat{\lambda}_{\eta,\infty} \sim \hat{\lambda}_{D,\infty} \sim S_{L_\perp}^{-3/4}. \tag{63}$$

Since $f_D > f_\eta$ for both models, $\hat{\lambda}_{D,i} > \hat{\lambda}_{\eta,i}$ for all $i < \infty$, and $\hat{\lambda}_{\eta,\infty}$ may be considered the final dissipation scale for the cascade. This scale is the same as the Kolmogorov (1941) scale that one expects as the dissipation scale in the GS95 model, i.e. for MHD turbulence without scale-dependent dynamic alignment. This reflects the fact that there is a lower limit on alignment imposed by the disruption process. This dissipation scale is the key testable prediction of our model for the disruption range. Encouragingly, Beresnyak (2014) found that in numerical simulations of RMHD turbulence, the dissipation scale was very close to the scale $\hat{\lambda}_{\eta,\infty}$.

6.3 Coarse-grained spectrum

We will now proceed to estimate the effective spectral index of the turbulent fluctuations in the disruption range. Namely, we will examine the amplitudes just above and just below the disruption scales to bound the effective scaling exponent in the disruption range.

The 'lower amplitude', just below the ith disruption, scales as (cf. equation 54)

$$\delta\hat{z}_{i,-} \sim \hat{\lambda}_{D,i}^{1/3}. \tag{64}$$

As $i \to \infty$, $\delta\hat{z}_{\infty,-} \sim S_{L_\perp}^{-1/4}$. These lower amplitudes, defined only on the coarse-grained set of scales $\hat{\lambda}_{D,i}$, define the lower envelope of the second-order structure function (or spectrum).

The 'upper amplitude', just above the ith disruption, scales as (cf. equation 55)

$$\delta\hat{z}_{i,+} \sim \hat{\lambda}_{D,i-1}^{1/3}\left(\hat{\lambda}_{D,i}/\hat{\lambda}_{D,i-1}\right)^{\zeta_2^\perp/2}. \tag{65}$$

Using the recursion relation equation (57), this may be written as

$$\delta\hat{z}_{i,+} \sim \hat{\lambda}_{D,i}^{(1/3-\zeta_2^\perp/2)(1+4f_D/3)^{-1}+\zeta_2^\perp/2} S_{L_\perp}^{-f_D(1/3-\zeta_2^\perp/2)(1+4f_D/3)^{-1}}. \tag{66}$$

In the MS17/B06 model, this is

$$\delta\hat{z}_{i,+}^{MS} \sim \hat{\lambda}_{D,i}^{3/5} S_{L_\perp}^{1/5}, \tag{67}$$

while in the CSM15 model,

$$\delta\hat{z}_{i,+}^{CSM} \sim \hat{\lambda}_{D,i}^{0.68} S_{L_\perp}^{0.26}. \tag{68}$$

As $i \to \infty$, $\delta\hat{z}_{\infty,+} \sim S_{L_\perp}^{-1/4}$ for both models, the same as the lower amplitudes. The upper amplitudes, defined on the coarse-grained set of points $\hat{\lambda}_{D,i}$, determine the upper envelope of the second-order structure function. Between disruptions, the fluctuations dynamically align and have the corresponding $\delta\hat{z} \propto \hat{\lambda}^{\zeta_2^\perp/2}$ scaling. A schematic for the idealized second-order structure function is shown in Fig. 4. It consists of segments with the scaling $\zeta_2^\perp$, joined by discontinuous jumps at each disruption scale $\hat{\lambda}_{D,i}$. In reality, the true structure function will be continuous and lie between the upper and lower envelopes.

The effective scaling of the second-order structure function is therefore bounded above by $\hat{\lambda}^{6/5}$ (MS17/B06, equation 67) or $\hat{\lambda}^{1.3}$ (CSM15, equation 68), and below by $\hat{\lambda}^{2/3}$ (equation 64). Using the usual correspondence between the second-order structure function and the spectrum, we expect the effective spectral index in the disruption range to be between $-5/3$ and -2.3 (CSM15) or $-11/5$

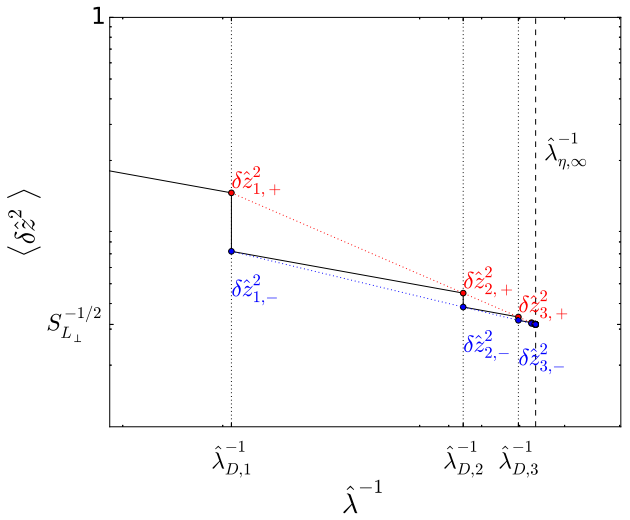

Figure 4. Schematic showing the idealized form of the second-order structure function in the disruption range (black solid line). Also shown are the upper amplitudes (66) as red points, lower amplitudes (64) as blue points and the upper and lower envelopes as red and blue dotted lines, respectively. The first three disruption scales are marked with vertical dotted lines, and the final dissipation scale $\hat{\lambda}_{\eta,\infty}$ (63) is marked with a vertical dashed line. We stress that the true structure function will be continuous and somewhere between the upper and lower envelopes.

(MS17/B06) in this range[9]. This is significantly steeper than the $-3/2$ in the free alignment range, despite the fact that between disruptions, there is scale-dependent alignment of fluctuations in a similar way to the primary cascade. However, to measure such a scaling unambiguously, one would likely need extremely high $S_{\mathrm{L}_\perp}$, high enough to have a good scale separation between $\hat{\lambda}_{\mathrm{D},1} \sim S_{\mathrm{L}_\perp}^{-4/7} \sim S_{\mathrm{L}_\perp}^{-0.6}$ and $\hat{\lambda}_{\eta,\infty} \sim S_{\mathrm{L}_\perp}^{-3/4}$. Thus, to test our model for the disruption range, it is potentially more productive to determine the scaling of the dissipation scale $\hat{\lambda}_{\eta,\infty}$, comparing it to the $S_{\mathrm{L}_\perp}^{-3/4}$ scaling given in equation (63).

It is perhaps worth commenting on how one might expect the scaling of the traditional alignment angles based on ratios of structure functions involving angles between different RMHD fields (Beresnyak & Lazarian 2006; Mason et al. 2006) to change in the disruption range. Because there is a physical lower limit to the alignment angle of turbulent structures in this range, these alignment measures will likely have a shallower scaling exponent at scales below $\hat{\lambda}_{\mathrm{D},1}$. Shallower scaling exponents for these measures were indeed observed at the smallest scales in the numerical simulations of both Perez et al. (2012, 2014) and Beresnyak (2012).

7 DISCUSSION

The dynamic-alignment models of strong Alfvénic turbulence due to B06, CSM15 and MS17 all predict that, as turbulent structures cascade to smaller scales, the vector fluctuations within them progressively align, and the structures become progressively more sheet-like and anisotropic within the perpendicular plane. In this paper, inspired by the recent work on the disruption of forming current sheets by Uzdensky & Loureiro (2016), we have found that these sheet-like structures are destroyed by reconnection below a certain scale $\hat{\lambda}_{\mathrm{D}}$. This disruption process occurs in two stages: linear growth of a tearing instability with multiple islands, and then collapse of the X-points between these islands into thin current sheets, which reconnect until the original structure has been destroyed. This means that the linear growth rate must be large compared to the cascade rate of the turbulence in order for the structures to be disrupted. To estimate the time-scales involved, we have used scalings from the turbulence models of MS17 and CSM15. Qualitatively, these models give similar results, although quantitatively the predicted scalings are slightly different.

We find that there is a critical scale $\hat{\lambda}_{\mathrm{D}} \sim S_{\mathrm{L}_\perp}^{-0.6}$, below which the turbulent structures are disrupted (see Section 5). This means that the turbulence theories that rely on dynamic alignment can only be expected to give accurate predictions at scales above $\hat{\lambda}_{\mathrm{D}}$. At $\hat{\lambda}_{\mathrm{D}}$, the turbulent cascade is effectively reset to unaligned structures, which can now cascade to smaller scales and again become progressively more sheet like and aligned. We show that they are recursively disrupted at a sequence of smaller scales $\hat{\lambda}_{\mathrm{D},i}$, with $i = 2, \ldots, \infty$ (see Section 6.1). We place bounds on the effective spectral index in the 'disruption range' below $\hat{\lambda}_{\mathrm{D}}$, and show that the effective spectral index is between $-5/3$ and -2.3, significantly steeper than the approximately $-3/2$ spectral index above $\hat{\lambda}_{\mathrm{D}}$ (see Section 6.3). However, a very large $S_{\mathrm{L}_\perp}$ is needed to detect a reliable power law in this range.

The disruptions get progressively closer to each other in scale as i increases, and in the limit $i \to \infty$ the turbulent fluctuations reach a final dissipation scale $\hat{\lambda}_{\eta,\infty} \sim S_{\mathrm{L}_\perp}^{-3/4}$ (see Section 6.2). This is a smaller scale than the dissipation scale predicted by the dynamic-alignment theories (B06; CSM15; MS17), and is identical to the Kolmogorov (1941) scale that one would expect for turbulence with a $-5/3$ spectrum (i.e. in the absence of dynamic alignment). This is despite the fact that the spectral index above $\hat{\lambda}_{\mathrm{D}}$ in our model is approximately $-3/2$ typical of the dynamic-alignment theories, and that between disruptions, there is scale-dependent alignment: effectively, the disruption process imposes a physical lower limit on the alignment angle. Thus, our argument that sheet-like structures are disrupted by reconnection below $\hat{\lambda}_{\mathrm{D}}$ might explain the discrepancy between the measured $-3/2$ spectrum in numerical simulations (Perez et al. 2014), and the seemingly opposing evidence that the dependence of the dissipation range on viscosity or resistivity[10] is much better described by the Goldreich-Sridhar/Kolmogorov scaling (Beresnyak 2014). Effectively, both sets of measurements are correct, but neither tells the 'full story': at large scales, dynamic alignment does occur, but at sufficiently small scales, the sheet-like structures become unstable, which limits the alignment, steepens the spectrum and forces the dissipation scale to have the Kolmogorov scaling. The scaling of $\hat{\lambda}_{\eta,\infty}$ is the key prediction of our model that is testable in currently feasible numerical simulations.

There are many improvements possible to the simple model of the disruption process and of the 'disruption range' that we have proposed here. First, we have neglected the effects of shear and viscosity on the stability of current layers (Chen & Morrison 1990a,b). Secondly, our conjectures about the turbulence below $\hat{\lambda}_{\mathrm{D}}$ are rather simple: we completely ignore the intermittency in this range, and do not take into account anything about the specific nature of the

[9] It might be worth mentioning in this context the results of Beresnyak (2017) and Kowal et al. (2017), who observed in 3D numerical simulations that reconnecting sheets generate turbulence that seems to agree with the GS95 scalings, and also the results of Huang & Bhattacharjee (2016), who performed a different simulation of reconnection-driven turbulence and found turbulence with a perpendicular spectral index of -2.1 to -2.3.

[10] All relevant simulations were done with equal viscosity and resistivity.

'flux-rope-like' structures produced by the tearing instabilities, apart from conjecturing a limit on their anisotropy in the perpendicular plane. Thirdly, we ignore any potential dissipation by the reconnection process; this may steepen the spectral index in the disruption range. Finally, in many situations (including the solar wind), kinetic scales will intervene at some point in the collapse process, significantly altering the dynamics. Nevertheless, we expect the idea that the sheet-like structures produced by dynamically aligning turbulence will eventually reconnect and destroy themselves is robust, even in kinetic systems, and provides an interesting link between inertial-range intermittent turbulent structures and magnetic reconnection.

ACKNOWLEDGEMENTS

We thank A. Beresnyak and N. Loureiro for useful conversations, and the referee, D. Uzdensky, for helping us improve the manuscript. While this manuscript was in an advanced stage of preparation, we became aware that a similar calculation of the disruption scale of sheet-like structures in Alfvénic turbulence (our equation 51) was concurrently being done by N. Loureiro and S. Boldyrev (Loureiro & Boldyrev 2016). We are grateful to N. Loureiro for alerting us to this work. The work of AM and BDGC was supported by National Aeronautics and Space Administration grant NNX15AI80G and National Science Foundation grants PHY-1500041 and AGS-1258998. AM was additionally supported by NSF grant AGS-1624501. The work of AAS was supported in part by grants from UK Science and Technology Facilities Council and Engineering and Physical Sciences Research Council. AM and AAS would like to acknowledge the hospitality of the Wolfgang Pauli Institute, Vienna, where the idea behind this work was first conceived.

REFERENCES

Beresnyak A., 2012, MNRAS, 422, 3495
Beresnyak A., 2014, ApJ, 784, L20
Beresnyak A., 2015, ApJ, 801, L9
Beresnyak A., 2017, ApJ, 834, 47
Beresnyak A., Lazarian A., 2006, ApJ, 640, L175
Bhattacharjee A., Huang Y.-M., Yang H., Rogers B., 2009, Phys. Plasmas, 16, 112102
Boldyrev S., 2006, Phys. Rev. Lett., 96, 115002 (B06)
Bruno R., Carbone V., 2013, Living Rev. Sol. Phys., 10, 2
Chandran B. D. G., Schekochihin A. A., Mallet A., 2015, ApJ, 807, 39 (CSM15)
Chandrasekhar S., 1961, Hydrodynamic and Hydromagnetic Stability. Oxford Univ. Press, Oxford
Chen C. H. K., 2016, J. Plasma Phys., 82, 535820602
Chen X., Morrison P., 1990a, Phys. Fluids B, 2, 495
Chen X., Morrison P., 1990b, Phys. Fluids B, 2, 2575
Chen C. H. K., Mallet A., Yousef T. A., Schekochihin A. A., Horbury T. S., 2011, MNRAS, 415, 3219
Chen C. H. K., Mallet A., Schekochihin A. A., Horbury T. S., Wicks R. T., Bale S. D., 2012, ApJ, 758, 120
Coppi B., Galvao R., Rosenbluth M., Rutherford P., Pellat R., 1976, Sov. J. Plasma Phys., 2, 533
Elsasser W. M., 1950, Phys. Rev., 79, 183
Furth H. P., Killeen J., Rosenbluth M. N., 1963, Phys. Fluids, 6, 459
Goldreich P., Sridhar S., 1995, ApJ, 438, 763
Goldreich P., Sridhar S., 1997, ApJ, 485, 680
Harris E. G., 1962, Nuovo Cimento, 23, 115
Horbury T. S., Forman M., Oughton S., 2008, Phys. Rev. Lett., 101, 175005
Huang Y.-M., Bhattacharjee A., 2016, ApJ, 818, 20
Kolmogorov A., 1941, Dokl. Akad. Nauk SSSR, 30, 301
Kowal G., Falceta-Gonçalves D. A., Lazarian A., Vishniac E. T., 2017, ApJ, 838, 91
Loureiro N. F., Boldyrev S., 2016, preprint (arXiv:1612.07266)
Loureiro N. F., Cowley S. C., Dorland W. D., Haines M. G., Schekochihin A. A., 2005, Phys. Rev. Lett., 95, 235003
Loureiro N. F., Schekochihin A. A., Cowley S. C., 2007, Phys. Plasmas, 14, 100703
Loureiro N. F., Uzdensky D. A., Schekochihin A. A., Cowley S. C., Yousef T. A., 2009, MNRAS, 399, L146
Loureiro N. F., Samtaney R., Schekochihin A. A., Uzdensky D. A., 2012, Phys. Plasmas, 19, 042303
Mallet A., Schekochihin A. A., 2017, MNRAS, 466, 3918 (MS17)
Mallet A., Schekochihin A. A., Chandran B. D. G., 2015, MNRAS, 449, L77
Mallet A., Schekochihin A. A., Chandran B. D. G., Chen C. H. K., Horbury T. S., Wicks R. T., Greenan C. C., 2016, MNRAS, 459, 2130
Mason J., Cattaneo F., Boldyrev S., 2006, Phys. Rev. Lett., 97, 255002
Oughton S., Dmitruk P., Matthaeus W. H., 2004, Phys. Plasmas, 11, 2214
Parker E. N., 1957, J. Geophys. Res., 62, 509
Perez J. C., Mason J., Boldyrev S., Cattaneo F., 2012, Phys. Rev. X, 2, 041005
Perez J. C., Mason J., Boldyrev S., Cattaneo F., 2014, ApJ, 793, L13
Podesta J. J., 2009, ApJ, 698, 986
Pucci F., Velli M., 2014, ApJ, 780, L19
Rutherford P. H., 1973, Phys. Fluids, 16, 1903
Samtaney R., Loureiro N. F., Uzdensky D. A., Schekochihin A. A., Cowley S. C., 2009, Phys. Rev. Lett., 103, 105004
Schekochihin A. A., Cowley S. C., Dorland W., Hammett G. W., Howes G. G., Quataert E., Tatsuno T., 2009, ApJS, 182, 310
She Z.-S., Waymire E. C., 1995, Phys. Rev. Lett., 74, 262
Shebalin J. V., Matthaeus W. H., Montgomery D., 1983, J. Plasma Phys., 29, 525
Strauss H. R., 1976, Phys. Fluids, 19, 134
Sweet P. A., 1958, in Lehnert B., ed., Proc. IAU Symp. 6, Electromagnetic Phenomena in Cosmical Physics. Cambridge Univ. Press, Cambridge, p. 123
Tenerani A., Velli M., Pucci F., Landi S., Rappazzo A. F., 2016, J. Plasma Phys., 82, 535820501
Uzdensky D. A., Loureiro N. F., 2016, Phys. Rev. Lett., 116, 105003
Uzdensky D. A., Loureiro N. F., Schekochihin A. A., 2010, Phys. Rev. Lett., 105, 235002
Verdini A., Grappin R., 2015, ApJ, 808, L34
Wicks R. T., Horbury T. S., Chen C. H. K., Schekochihin A. A., 2010, MNRAS, 407, L31
Zhdankin V., Uzdensky D. A., Perez J. C., Boldyrev S., 2013, ApJ, 771, 124
Zhdankin V., Boldyrev S., Uzdensky D. A., 2016, Phys. Plasmas, 23, 055705

This paper has been typeset from a TEX/LATEX file prepared by the author.